energies

MDPI

Review

Modeling of Electrodynamic Phenomena in an Ultra-Rapid Inductive–Dynamic Actuator as Applied to Hybrid Short-Circuit Breakers—A Review Study

Damian Hallmann [1], Piotr Jankowski [1,*], Janusz Mindykowski [1], Kazimierz Jakubiuk [2], Mikołaj Nowak [2] and Mirosław Woloszyn [2]

[1] Department of Marine Electrical Power Engineering, Gdynia Maritime University, 81-225 Gdynia, Poland
[2] Department of Electrical and High Voltage Engineering, Faculty of Electrical and Control Engineering, Gdansk University of Technology, 80-233 Gdansk, Poland
* Correspondence: p.jankowski@we.umg.edu.pl

Abstract: This article is a study of the research development of electrodynamic phenomena occurring in ultra-fast electrodynamic drives. These types of linear drives are among the fastest, not only because of the huge accelerations achieved, but, above all, because of the extremely short reaction time. For this reason, electrodynamic drives are used in hybrid short-circuit breakers. The phenomena occurring in this type of drive are actually magneto-thermo-elastic in nature, but the coupling of these phenomena should be considered weak if the criteria for repeatable operation in a hybrid circuit breaker system are met. The authors have been researching this type of drive for many years through not only experimental studies, but also primarily simulation studies developing models of such drives. The authors present the history of the development starting from the first works of Thomson, and Kesserling and ending with the most current models, including mainly their own. This article presents mainly works studying electrodynamic phenomena. Thermal and mechanical phenomena were comprehensively presented by the authors in previous papers.

Keywords: hybrid circuit breaker; electrodynamic actuator; ultra-rapid displacement; model in Maxwell environment; experimental research

Citation: Hallmann, D.; Jankowski, P.; Mindykowski, J.; Jakubiuk, K.; Nowak, M.; Woloszyn, M. Modeling of Electrodynamic Phenomena in an Ultra-Rapid Inductive–Dynamic Actuator as Applied to Hybrid Short-Circuit Breakers—A Review Study. *Energies* **2022**, *15*, 9394. https://doi.org/10.3390/en15249394

Academic Editor: Oscar Barambones

Received: 31 October 2022
Accepted: 3 December 2022
Published: 12 December 2022

1. Introduction

The induction–dynamic drive (IDD) is considered the fastest physically existing actuator, since the instantaneous acceleration of the moving element can reach hundreds of thousands of g (Earth acceleration). In the work presented, the authors tried to show the historical development of mathematical modeling of electromagnetic phenomena of this actuator with progressive reduction in successive simplifications.

Concerning processes occurring in electrodynamic drives, previous papers on both using an analytical approach [1,2] and numerical–analytical approach [3,4] assumed several additional simplifications, the most important of which were: assumption of cylindrical symmetry of the system, simplification of the analysis to the skin layer only, omitting the influence of disc motion on IDD parameters, and, finally, assuming a priori knowledge of the excitation coil current (Thomson) or the distribution of the current radial density in the disc. Concerning these assumptions, the last important reports using the numerical approach [5–17] did not analyze all magneto-thermo-elastic phenomena or also assumed current extortion or quasi-steady state voltage.

Analytical–numerical IDD models created by the authors in [18] did not contain most of these simplifications, but also limited the research to systems characterized by ideal cylindrical symmetry. Moreover, the non-stationary model (taking into account the influence of the disc motion treated as a rigid body on the parameters of the system) requires long calculation times, even with low discretization of elements of the IDD model.

Therefore, the authors have established the following scientific objectives resulting from the current state of research related to the IDD study:

- Development of tests of IDD drive properties in order to determine critical parameters using and modifying (extending) our own models of electromagnetic and mechanical phenomena;
- Elaboration and construction of a new measurement system (with better metrological properties) with a physical IDD model allowing for additional verification of model test results;
- Construction of new numerical models using the FEM technique (assuming real voltage extortion), describing magneto-elastic and thermal phenomena in both 2D and 3D options, enabling future design of drives that take into account the lack of any symmetry.

2. Inductive Dynamic Drive (IDD)

The inductive–dynamic propulsion system is composed of a coil supplied from a battery of capacitors and a disc magnetically coupled with it (Figure 1a). The inductive–dynamic drive is a linear actuator in the electrodynamic drive class. The term "linear" refers mainly to the linear motion with which the drive displaces the moving element. In practice, electrodynamic drives are electrically and magnetically linear because they do not contain ferromagnetic elements. The phrase "inductive–dynamic" is related to the phenomenon of induction of eddy currents in a secondary element of this drive called a disc or a ring (Figure 1a). The phenomenon of dynamic rejection of a conductive element (disc) magnetically coupled with the coil as a result of generating an impulse magnetic field was first presented by Thomson. Therefore, researchers of this actuator commonly use the following terms in the wide literature: "Thomson's phenomenon" or "Thomson's coil" [6,8,9,19]. One of the conditions for obtaining a high force in a short time is a small value of resistance of the coil circuit and of internal resistance of the voltage source. Therefore, the most often used as a power supply system is a capacitor battery. Inductive and dynamic drive (IDD) is used in many technical devices, in which it is required to achieve rapid displacement of a moving element with almost immediate reaction from the moment of initiation of this movement. Thus, the IDD has gained an advantage over spring, electromagnetic, and even explosive drives. Another fundamental feature that characterizes IDD is its repeatability of operation and long-term reliability (provided that the correct parameters of all its components are determined). The above advantages of the IDD resulted in its taking over from other types of drives (e.g., spring ones) in many circuit breakers, especially in the so-called hybrid circuit breakers (Figure 1b) of both DC [20–26] and AC used in synchronous switching-off [27–33]. The interest of the authors in the study of this type of drive is mainly related to their application in the class of circuit breakers considered [30,32–41]. The authors' noted works can be divided into those focusing on the study of electromagnetic [35,40], mechanical [34,38], and thermal [41] phenomena of the drive. References [36–38] present the development of measurement systems that allow the experimental determination of the basic drive quantities. Finally, articles [30,39] describe the results of tests on hybrid switches in which the basic element is the actuator. More detailed descriptions can be found later in the article, where most of the papers [30–41] are further referenced.

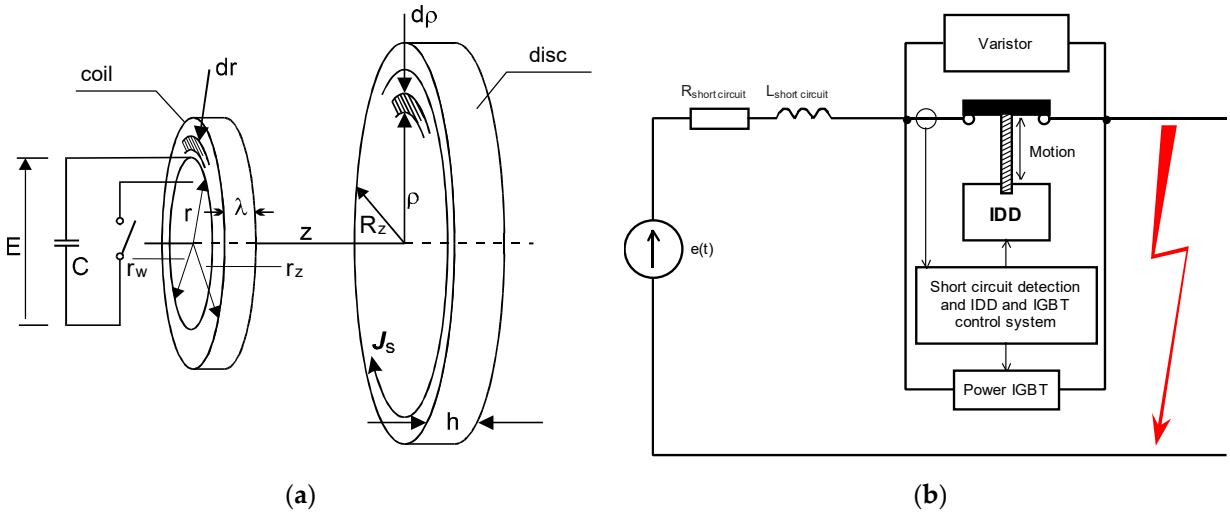

Figure 1. (**a**) Inductive–dynamic drive (IDD); (**b**) block diagram of hybrid circuit breaker. Where rw, rz, λ, Rz, h—coil and disc dimensions; Js—eddy current density; C, E—capacitance and initial voltage.

Owing to the use of IDD in hybrid circuit breakers, solutions [42–45] were developed which allow for arc-free switching-off of short-circuit currents. However, one of the conditions to achieve such a fast process of short-circuit current disconnection is to obtain a very short own time (approx. 20 μs—the time counted from the moment of giving the impulse (synchronous command) to the opening of the mechanical contact).

IDD-type drives are able to meet such strict requirements owing to the enormous momentary accelerations achieved, provided that such IDD parameters are selected that do not exceed critical values. The notion of critical values has been introduced in reference [46]; the exceedance of which may cause malfunction of the hybrid switch, or even its damage. The authors specify this term by an additional condition not to exceed such values of IDD parameters for which the coupling of occurring magneto-thermal-elastic phenomena should be considered strong. In such a situation, the system of equations describing the phenomena of magneto-thermal-elasticity in the form of [47–49] should be solved:

$$\begin{cases} \mu\nabla^2\mathbf{u} + (\lambda+\mu)\nabla(\nabla\cdot\mathbf{u}) - \frac{1}{\mu_m}\mathbf{B}_0\times\nabla\times(\Delta\mathbf{B}) = \rho\frac{\partial^2\mathbf{u}}{\partial t^2} + \beta\nabla T \\ \nabla^2 T = \frac{1}{h}\frac{\partial T}{\partial t} + \eta\nabla\cdot\left(\frac{\partial\mathbf{u}}{\partial t}\right) - \frac{P'}{\lambda_c} \\ \nabla^2\Delta\mathbf{B} - \gamma\mu_m\frac{\partial\Delta\mathbf{B}}{\partial t} = -\gamma\mu_m\nabla\times(\mathbf{v}\times\mathbf{B}_0) \end{cases} \quad (1)$$

where $\mathbf{B}_0$—vector of primary induction; $\Delta\mathbf{B}$—increment of magnetic induction caused by body deformation; $\mathbf{u}$, $\mathbf{v}$—displacement and velocity of the medium; λ, μ—Lame coefficients; γ—conductivity; P'—volumetric density of electric power; μ_m—magnetic permeability; ρ—mass density; η—thermo-elasticity coefficient; λ_c—thermal-conductivity coefficient; and h—thermal diffusivity.

Examples for solving this kind of problem in conditions of strong coupling of these three phenomena can be found in papers analyzing the process of disintegration (explosion) of wires as a result of high impulse currents [49–51]. The purpose of the analyses carried out is the disintegration of conductive wires (fuses) in contrast to the phenomena which are the subject of the authors' research. Namely, critical parameters determined for the IDD not only cannot lead to permanent destruction of any of the drive components (coil, disc), but even elastic deformations mainly of the disc must be limited to small values in order to ensure proper cooperation with the hybrid switch. Therefore, in most papers in which not only electromagnetic but also thermal and mechanical phenomena were analyzed, it was assumed that the conditions under which the IDD should operate justify treating the coupling between these phenomena as a weak interaction [3,4,52].

3. Measurement of Basic Quantities Characterizing the Properties of the Induction–Dynamic Drive

In order to verify the models of electrodynamic actuators, the authors designed and built a new measuring system that allows direct registration of the coil current and displacement of the disc [36,37]. In relation to the previously used measurement system [18] the goal of the new one was, among other features, to minimize the external vibrations of the system that could introduce additional disturbances both in the course of the disc motion and in the measurement sensors (Figure 2). An additional connector based on the IGBT transistor (previously a thyristor) was constructed to increase the dynamic state of the transient in the capacitor discharging system (Figure 2b). The registration of the coil current, similarly as in the previous system, was based on a measuring shunt characterized by a very low inductance necessary to register currents whose rise steepness may exceed 5 kA/μs. Therefore, a new bifilar resistive sensor was used.

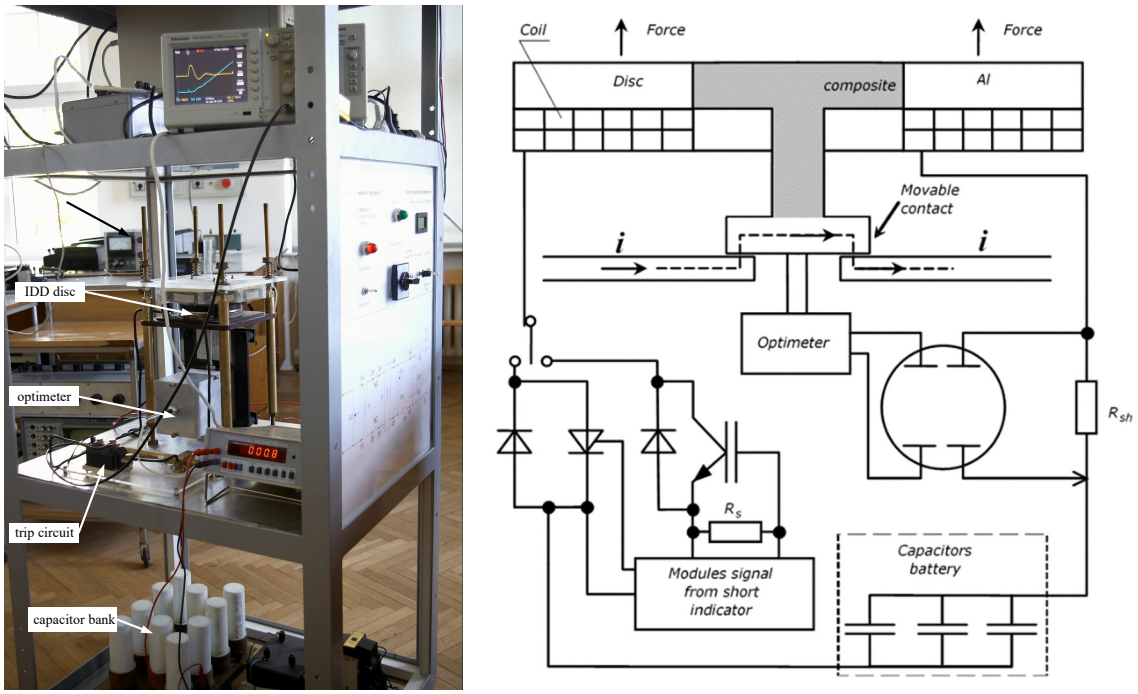

(**a**) (**b**)

Figure 2. A photo (**a**) and scheme (**b**) of a measuring system for testing physical models of electrodynamic drives.

In [18], a potentiometric sensor was used for displacement measurements (which proved to be unreliable for increasing accelerations of a moving disc), and an optical sensor based on a photosensitive ruler based on photodiodes (p-i-n). The light sensor's diaphragm reveals (during the movement of the disc) a photosensitive matrix, which was obtained by connecting strips (photodiodes) in parallel (Figure 3). However, during the research period (for various IDD physical models) some measurement instabilities were noticed, which could be mainly explained by using a halogen lamp with too much power, which caused the temperature to increase in a closed (shielded from the pulsed magnetic field) sensor. On the other hand, after the time the temperature stabilized, it reached a value above 60 °C, which could have influenced the increase in thermal noise. It should also be emphasized that in the original sensor no tests were performed with different light sources and loads (resistors). In addition, to obtain the displacement function vs. time, the sensor's output characteristics were derived from unprocessed data (raw data) without mathematical data processing (filtration). Therefore, for the new IDD measurement system, optical sensor tests were carried out in order to select the optimal (among the possessed)

light sources and the resistor loading the sensor, on which the recorded voltage depending on the shift of the sensor's diaphragm [37]. The main purpose of the photoelement research was to select the lighting and load resistance of this sensor, for which the determined static characteristics were characterized by very good linearity and sensitivity in a given range of diaphragm shift. The sensitivity of the photoelement (photodiode) is normally defined as the ratio of the output current or voltage (in the considered case the voltage across the load resistance) to the optical power of the input signal [53]. However, from the point of view of the registration characteristics of the output voltage as a function of displacement of the shutter (disc), the sensitivity was defined as the ratio of the voltage increment to the displacement increment ($\Delta v/\Delta x$).

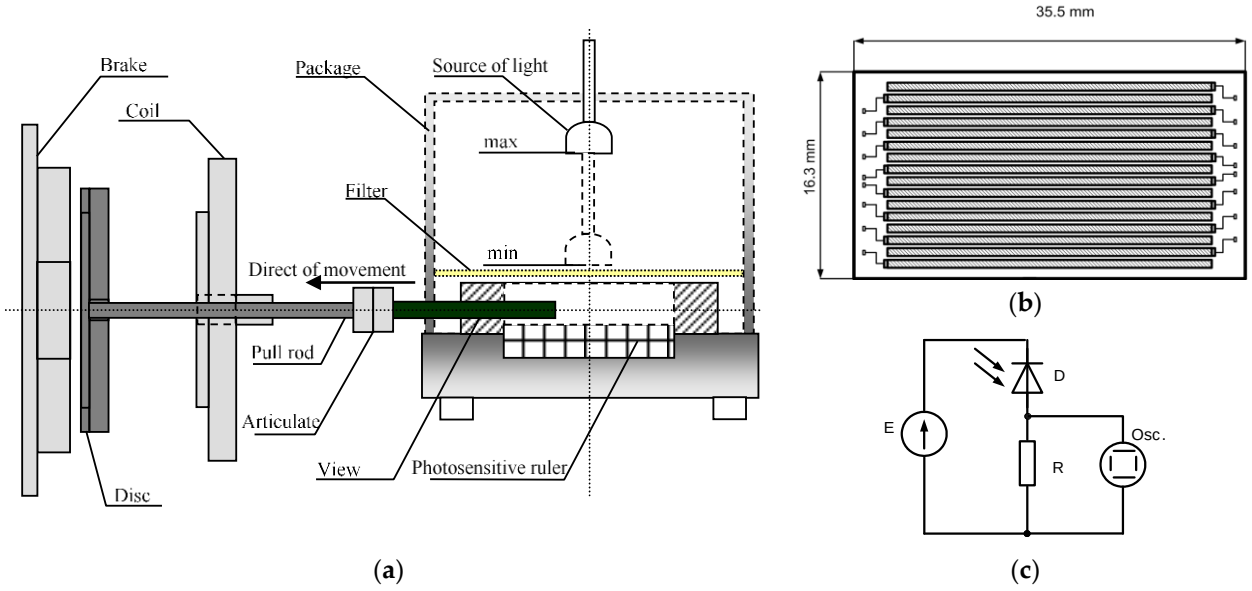

Figure 3. Photoelement (**a**) view of construction, (**b**) matrix structure of photosensitive ruler, and (**c**) photodiode system.

In [37], in the first stage, tests were carried out to determine the static characteristics of the optical sensor in both photovoltaic and photoconductive mode for different values of the surface of the exposed matrix determined by the distance of the diaphragm from the point where the shutter completely covered the matrix. The characteristics obtained allow for a preliminary determination of the load range that ensure good working conditions from the point of view of both linearity and sensitivity. The output static characteristics were also determined in two systems, i.e., in the photodiode and photovoltaic cell system, although in the case of a photovoltaic cell, we can already observe a much lower output signal, which would have to be amplified when using this system in the sensor.

In spite of this disadvantage, the output characteristics in both systems were determined to compare their linearity, and especially the insensitivity threshold, which was observed at the beginning of the displacement. As the source of light, three halogen lamps with 50, 20, and 3.5 W power were used, characterized by continuous spectrum, along with a fluorescent lamp (band spectrum) with 14 W electrical power. As expected, with the given load resistance, the best sensitivity was characterized by the characteristics for the highest power of the light sources, with the fluorescent lamp having the worst performance for linearity. For the chosen source of light and load, the measurement range after cutting off the insensitivity zone and the saturation zone had a value from 3 to 8 mm, i.e., a displacement sufficient for the nature of the hybrid switch [28,29,42,45]. On the other hand, low sensitivity may lead to too high an impact of (external) disturbances on the measurement result. Based on the equivalent scheme of the photoelement, the output voltage/current functions can be determined from the optical radiation power argument, which in the case of the photodiode system is a linear function (up to saturation corresponding power supply

voltage), and for the photovoltaic cell, the output voltage (in the unloaded condition) is a logarithmic function [53]. However, it is necessary to emphasize the specificity of the sensor in the form of the exposed matrix (photosensitive ruler), where we do not have the guarantee of the same features of strips of photosensitive element (consisting of sixteen strips) over its entire length (Figure 3). In addition, it must be emphasized that the halogen bulb at a working distance from the photosensitive ruler (6 cm) is not an isotropic source and not all fragments of the exposed photosensitive ruler are equally illuminated. Therefore, we can describe the approximation to the linearity of the characteristics obtained in the photodiode system, which in turn forces us to use the conversion of the measurement course (output characteristics) to the course of the displacement.

As mentioned before, a resistive Megatron linear displacement sensor was used to record the displacement at small initial capacitor energy (E < 40 J). The comparison of the waveforms obtained from the optical and potentiometric sensors yielded very good results. However, to carry out the validation of the modified sensor, it was necessary to construct a system that allow for determining at least a few measurement points of the displacement characteristic with much higher initial energy of the capacitor (e.g., 6-fold increase). For this purpose, a simple inertia-less circuit (E-R) is used, closed with a connector whose one contact is a moving disc (Figure 25 in [37]). The moment of occurrence of the current pulse in the E-R circuit determined the time after which the disc traveled the distance to the second contact. With each "shot" (initiating disc motion by providing a gate pulse of the connector closing the coil circuit), the precise measurement of the distance between the disc and the second contact was changed and determined. In this way, it was possible to determine several points of the displacement characteristic and compare it with the characteristics obtained as a result of the conversion of the waveform recorded from the optical sensor. The differences (relative error) between the displacement characteristics obtained in this case for the considered initial energy (E = 245 J) did not exceed 4%. It should be emphasized that this method can be implemented owing to very good repeatability of the obtained currents and displacements for each "shot". Summarizing the results, it can be concluded that the modified optical sensor is suitable for recording dynamic displacements, and is additionally characterized by simplicity of construction and lower costs compared to other complex measurement systems used to record straight-line traffic. However, it should be underlined that the presented sensor records the movement of one point (in this case it is the center of the disc). Currently, ultra-fast cameras are used to record the movement of the disc, allowing for observation of the movement of the whole object, which allows for obtaining a course of displacement in time of each point marked on the disc. Currently, the latest measurement system (authors' system) is equipped with such a camera (Figure 4). Significant results (according to the authors) obtained with the use of an ultra-fast camera recording the movement of the entire disc are presented in [40]. Measurement of the basic quantities recorded in the measurement system discussed, i.e., current using a low inductance resistive shunt and displacement via an optical sensor, can be determined as a direct measurement. Reference [36] discusses the metrological classification of the most important quantities characterizing the induction–dynamic drive into those measured directly and indirectly. The indirect measurement is understood to be a result of a measured quantity that can be obtained by way of more or less complex mathematical operations on quantities measured directly (unprocessed raw data). In the case of displacement, the values of velocity and acceleration can be obtained by double differentiation. However, when attempting to differentiate the course obtained in the form of raw data, this operation results, as could be expected, in a large distortion due to even slight disturbances in displacement characteristics.

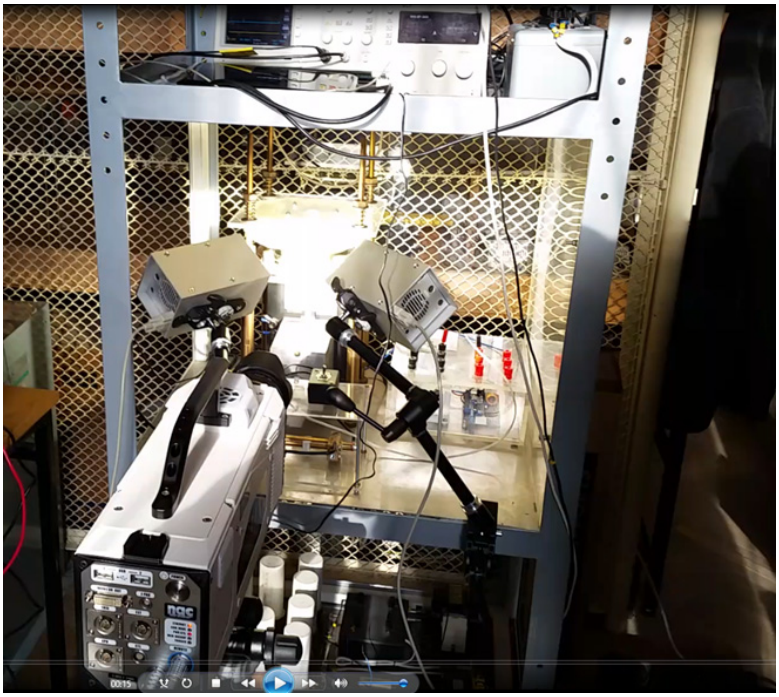

Figure 4. Photo of the station for measuring the movement of the disc using the ultra-fast video camera.

The source of interference may be the noise generated by the detector circuit (resistances), such as the already-mentioned thermal noise (Johnson's noise). It is worth noting that this noise is inversely proportional to the resistance, which additionally justifies the use of a high resistance (40 kΩ) in the photodiode power supply circuit. In addition to thermal noise, other types of interference are also known, such as shot-noise, generative–recombination noise, or also the so-called low-frequency noise 1/f, whose nature is not clearly defined, but according to [53] most probably results from the presence of impurities and network defects. One can also state that even recording using a digital oscilloscope introduces distortions when transmitting the signal measured from the oscilloscope registrator to computer. An example of the occurrence of these disturbances is not only the course of displacement obtained from the photooptical sensor, but also the current waveform in the RLC system. In general, it should be assumed that the disturbances appearing in the system of the photoelement used can be deterministic or random, both in the case of determination of the static output characteristics (for conversion) of the sensor, and in the registered course of the displacement. Therefore, in order that the final course of displacement as a function of time be subjected to further mathematical processing (double differentiation), and to obtain at least qualitatively reliable velocity and acceleration courses, the mean square approximation procedure was performed for both the static characteristics of the optical sensor and the dynamic displacement of the disc recorded by this sensor [36]. When determining the approximation functions, decisions should be made on how to measure the deviation and what kind of basic functions, the polynomial degree, and what number of measuring points should be used. As a measure of deviation, the commonly used mean square error was accepted. When choosing basic functions, one should be guided by minimizing the sensitivity to rounding errors. This type of function includes orthogonal functions. In the case studied, the orthogonal Gram functions were used. Formula (2) generates consecutive orthogonal polynomials of the k-th degree depending on the n-number of nodes. Measurement nodes x must be equidistant because they must be

reduced to the natural collection. The use of orthogonal basis functions allows for very simple determination of the coefficients of the approximate polynomial (3).

$$Pol\_Grama(x,k,n) = \sum_{s=0}^{k} [(-1)^s \cdot \frac{k!}{s! \cdot (k-s)!} \cdot \frac{(k+s)!}{s! \cdot k!} \cdot if[s > 0, \frac{\prod_{i=0}^{s-1}(x-i)}{\prod_{i=0}^{s-1}(n-i)}, 1]] \quad (2)$$

$$s_j = \sum_{i=0}^{n} (Pol\_Grama(i,j,n))^2 \; c_j = \sum_{i=0}^{n} (y_i \cdot Pol\_Grama(i,j,n)) \; wsp_j = \frac{(c_j)}{(s_j)} \quad (3)$$

This avoids complex transformations which, when using non-orthogonal base functions, can lead to large computational errors due to the limited representation of the number. In computing environments such as Mathcad and Matlab, the maximum representation of the number is 17 digits [54]. An important issue that had to be solved for obtaining the procedure to resolve the approximate polynomial was to determine the sufficient degree of the polynomial sought and the number of measuring points. In the approximation theory, it is assumed that with an increasing number of measurement points, we approach the expected value (assuming no systematic errors). In the case of recording the displacement waveform using an oscilloscope, 2500 measuring points are standard. However, the output characteristic is determined point by point using a micrometer screw, which is time-consuming; therefore, studies that try to determine a sufficient number of such points have been significant.

Because when determining the approximation function, we do not know the theoretical function sought, very often as the criterion for the best approximation determined from among the different numbers n and for various degrees of polynomials k, the smallest error of the mean square error is used. The research conducted by the authors [36,55] showed that the minimum mean square error should not be the only criterion for selecting the number of measuring points (or the degree of polynomial). The authors in [55] presented the test result determining the variation in the mean square deviation for the known theoretical function with the added disturbance as a function of the number of measuring points. It turned out that the smallest mean square deviation occurred for a very small number of measurement points at a large relative error. Of course, it should be emphasized that the mean square deviation is not determined in relation to the points on the theoretical curve, which in practice we do not know, only in relation to the measurement points.

As a consequence of the authors' experiences, the choice of both the polynomial degree and a sufficient number of measurement points of the static output characteristic was made on the basis of observations of the determined runs of the medium standard deviation and the maximum relative error. As a result of these tests, it was considered that the sixth degree polynomial using the Gram function is sufficient and the number of measurement points should not be fewer than 50 (Figure 5). The authors developed the approximation procedures using the Gram function in the Mathcad environment [36]. The flow chart for determining the filtered characteristic of displacement allowing for obtaining smooth velocity and acceleration functions of the disc is shown in Figure 6. In the first stage, the measurement points of the static characteristic of the optical sensor (Up(x)—voltage in the displacement function for at least 50 points) are determined, and as a next step this characteristic is approximated. Then, the dynamic movement of the disc (Up(t)—voltage as a function of time) is recorded, which is also approximated. Then, the filtered U_{approx} voltage function is converted to the actual displacement waveform as a function of time.

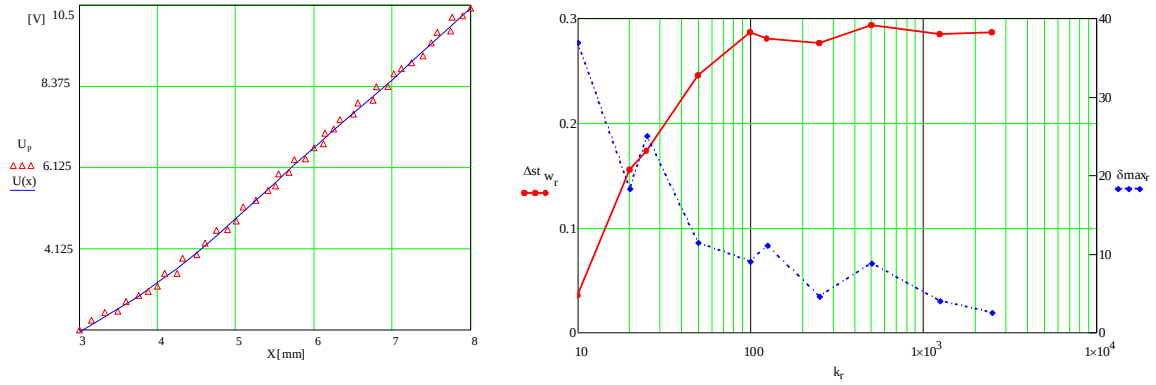

(**a**) (**b**)

Figure 5. (**a**) The output characteristic of the optical sensor (measurement and approximation); (**b**) the mean square error and the relative error in function ($k_r = n$) of the number of measuring points taken into account.

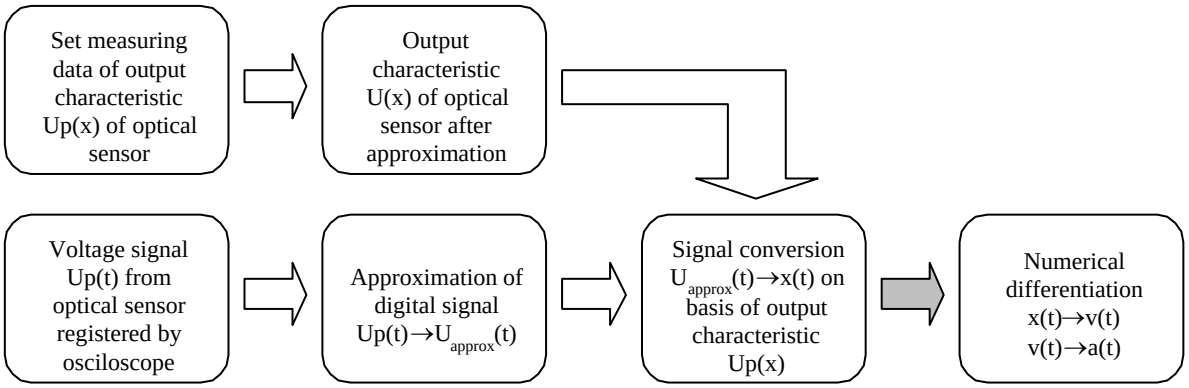

Figure 6. Block diagram of the procedure for determining the displacement waveform.

Finally, the trajectory of the displacement can be twice differentiated numerically. Differentiation was performed on the basis of a procedure that uses five neighboring points.

As can be seen in Figure 7b, the obtained velocity waveforms, in particular accelerations, indicate the vibrating nature of the actual displacement of the disc center or occurrence of the braking electrodynamic forces during the motion. At this stage of research, the generation of such forces was ruled out.

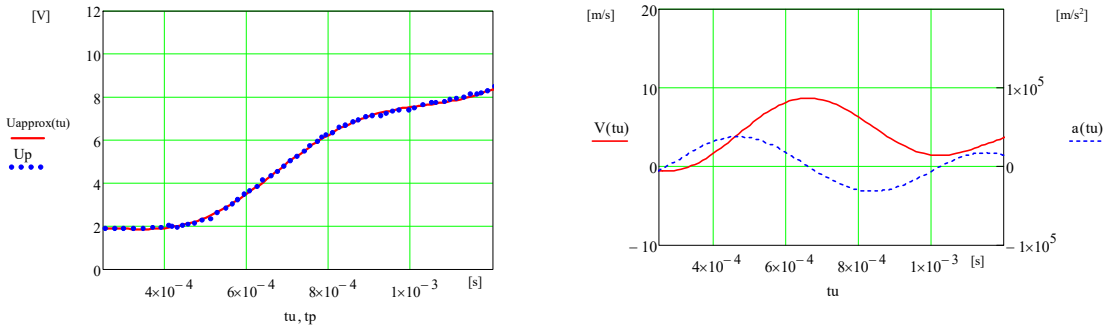

(**a**) (**b**)

Figure 7. (**a**) Displacement (measurement and approximation) before conversion; (**b**) differentiation of post-conversion displacement.

The authors observed the problem of the appearance of such forces during the movement as a result of later research using the new mechanical model described in [40].

4. Modeling of Electromagnetic Phenomena of the Induction–Dynamic Drive

4.1. Criticism of the Most Important Existing Models of Electromagnetic Phenomena in IDD

The first models describing electromagnetic phenomena taking place in IDD [1,2] used a purely circumferential approach based even on a one- or two-loop circuit [56,57], in which the primary circuit was a coil supplied from capacitor banks, often treated (in the model) as a sinusoidal voltage or current source. The secondary circuit (magnetically coupled to the original) of the RL-type represented disc parameters that were determined experimentally or analytically (with significant simplifications consisting in bringing the disc to the skin layer and assuming a constant current density in that layer). It should be emphasized that the experimental determination of fixed values of inductance and resistance of the disc (and coil) did not take into account the variability of these parameters as a function of time, which is the result of a pulsed non-stationary process. A separate issue was the analytical determination of the magnetic coupling coefficient, which even in the case of these simplifications was possible only if the IDD was characterized by cylindrical symmetry. The resultant axial force acting on the disc was determined on the basis of the above parameters and the coefficient determined experimentally. An additional problem is the fact that the secondary element (disc) moves, that is, the variability of these parameters in the function of not only the time but also the distance from the coil.

Since only a slight displacement of a few millimeters is significant for applications in hybrid switches; hence, the simplification often used was the assumption of no movement of the disc. The model for such an assumption is hereinafter referred to as stationary, in contrast to models called non-stationary, i.e., taking into account the effect of disc motion on electromagnetic quantities. In stationary models, disc motion was often calculated on the basis of the force determined for a fixed disc located at a distance from the coil.

These basic models gave satisfactory results for a very small range of free frequencies of the coil supply circuit (RLC) not exceeding 1 kHz. Their only advantage was the possibility of obtaining a simple solution using the analytical method. Figure 8 presents a block diagram that is an attempt to systematize the models used so far, which analyze in the narrower or wider range the electromagnetic phenomena (EM) in induction–dynamic drives (IDD).

With the increasing computing capabilities of computers, there began to develop the so-called *current filament methodology*, which is a circumferential approach to current distribution analysis in well-conducting bodies exhibiting symmetry [58–60]. This method assumes the discretization of the coil and disc into filaments in which a uniform distribution of current density can already be assumed. For these filaments, circuit parameters such as resistances, internal inductances, and mutual inductances are determined. The discretization method into current filaments described above was used in the work related to modeling unipolar generators [59] or electromagnetic launchers and the guns [58,60]. This approach was also used by the authors in [18] and further developed in the form of the electrodynamic model discussed in more detail below.

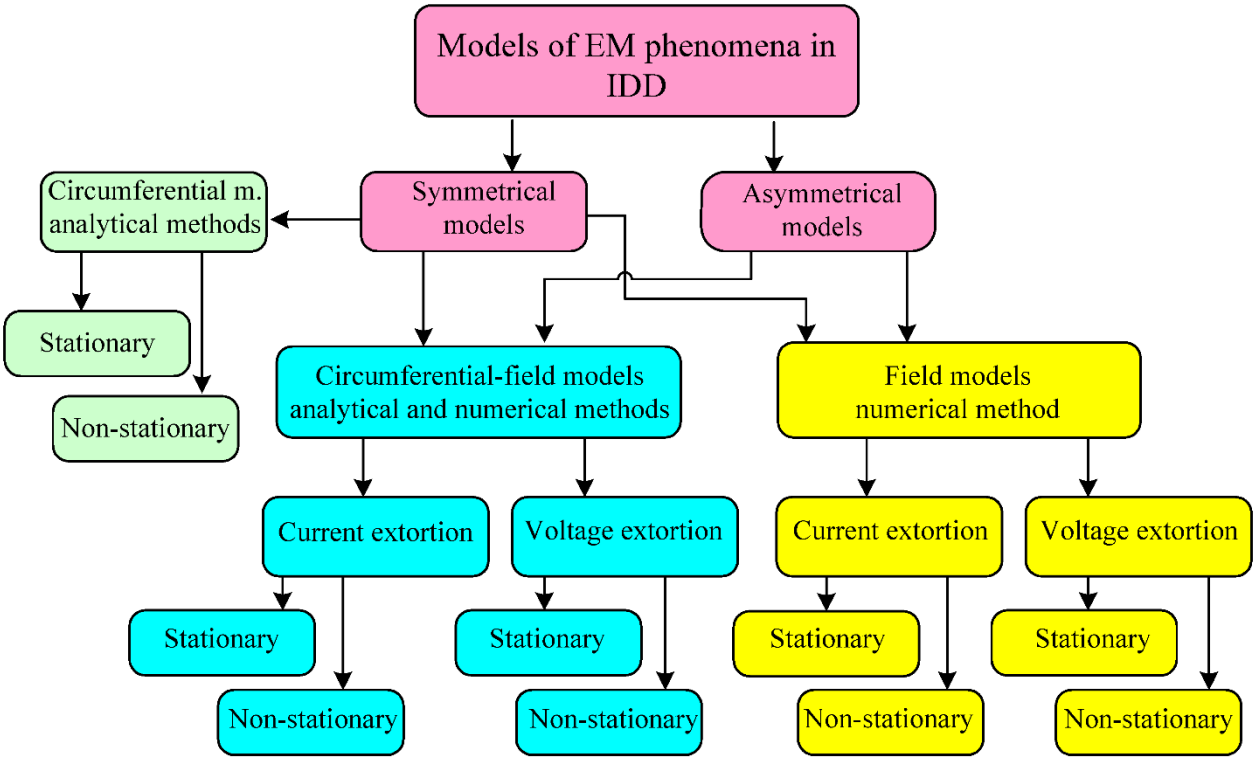

Figure 8. Ways of modeling electromagnetic phenomena in the induction–dynamic drive.

An attempt to analytically solve the problem from the circumferential-field perspective for a system with cylindrical symmetry was undertaken in [3,52]. The authors of these papers, in order to determine the equivalent inductance L_E of the coil–disc system, also used the method of current filaments performing a single-layer discretization of the disc. However, in order to obtain a solution to field equations, they had to make a number of simplifying assumptions, the more important of which are:

- Treating the disc as an infinite surface, which allowed for omitting the determination of the boundary condition;
- Occurrence of eddy currents only in the skin layer of the disc;
- Determination of the extortion current of the coil on the basis of the one-loop model, with constant equivalent L_E inductance determined by the single-layer disc discretization method.

Starting from Maxwell's equations (with displacement current being omitted) and taking into account the definition of magnetic vector potential:

$$\nabla \times \mathbf{B} = \mu_0 \mathbf{j}, \ \mathbf{B} = \nabla \times \mathbf{A} \tag{4}$$

The equation describing the magnetic field in the conductive region was obtained:

$$\nabla \times \nabla \times \mathbf{A} = \mu_0 \mathbf{j} \tag{5}$$

Equation (5) (after Coulomb calibration) in the cylindrical coordinate system and taking into account that both the vector **A** potential and the current density **j** have in this case cylindrical symmetry, only the angular component takes the form:

$$\frac{\partial^2 A_\Theta}{\partial \rho^2} + \frac{1}{\rho}\frac{\partial A_\Theta}{\partial \rho} - \frac{A_\Theta}{\rho^2} + \frac{\partial^2 A_\Theta}{\partial z^2} = -\mu_0 j_\Theta \tag{6}$$

In the currentless area, the magnetic field is described by the Laplace equation:

$$\frac{\partial^2 A_\Theta}{\partial \rho^2} + \frac{1}{\rho}\frac{\partial A_\Theta}{\partial \rho} - \frac{A_\Theta}{\rho^2} + \frac{\partial^2 A_\Theta}{\partial z^2} = 0 \tag{7}$$

For an analytical solution of Equation (7), the authors of [52] adopted the form:

$$A_\Theta(\rho, z) = \frac{\mu_0 N i(t) a}{2} \int_0^\infty J_1(ka) J_1(k\rho) e^{-kz} dk \tag{8}$$

where:

N is the number of coil turns with geometry simplified to the wire with radius a;
$i(t)$ is the sinusoidal current of the coil;
k, J_1 is the separation constant and Bessel first kind and first order function.

In [52], the concept of determining the vector potential as the sum of the potentials generated by the coil and the eddy currents of the disc was adopted:

$$A(\rho, z) = A_s(\rho, z) + A_e(\rho, z) \tag{9}$$

where $A_s(\rho, z)$ is the angular component of the vector potential of the coil (or eddy current) defined in Formula (8).

The vector potential from currents induced in the disc $A_e(\rho, z)$ was also obtained from Equation (8) after insertion of the relationship determining the current of the disc filament from the current density in the disc $j_s(r)$ in place of current i(t) (with the filament width dr and the thickness equal to the skin thickness, which in [52] was obtained assuming the lack of damping the coil current). In turn, instead of the radius a of the coil, the radius of the considered filament r is substituted, and then by integrating along the radius the vector magnetic potential [52] is obtained:

$$A_e(\rho, z) = \frac{\mu_0 \delta}{2\sqrt{2}} \int_0^\infty r j_s(r) dr \int_0^\infty J_1(kr) J_1(k\rho) dk \tag{10}$$

Considering that: $\mathbf{E} = -\frac{\partial \mathbf{A}}{\partial t}$ and

$$\mathbf{j} = \gamma \cdot \mathbf{E} \tag{11}$$

and taking into account the existence of only angular components of vector magnetic potential and current density, the following formula is obtained:

$$j = -\gamma \frac{\partial A}{\partial t} \tag{12}$$

By inserting (12) into the vector potential (9), the authors of [52] obtained the integral equation from which they determined the current density in the disc depending on the current of the coil. It should be noted that the coil current, despite its transient character, was treated in [52] as a harmonic function with a constant amplitude. On the basis of the current density in the disc, it was possible to determine the components of the vector potential (9) and then the components of the induction of the magnetic field acting on the disc, and on this basis, the force could be found.

The authors of [52] continued their theoretical work in [3] where a thin coil constituted a conductive ring with a width defined by the inner and outer radius. Similar as in the disc, it was assumed that the current of the coil (ring) flows only in the skin layer, with the hyperbolic distribution along the radius adopted for this current. The idea for determining eddy currents in the disc remained unchanged and was based on the determination of the sum of vector magnetic potentials separately from the coil and disc. Equation (11) has

been supplemented with a field component depending on the movement of the conducting environment:

$$\mathbf{j} = \gamma(\mathbf{E} + \mathbf{v} \times \mathbf{B}) \tag{13}$$

In this way, similar as that in [52], in the formulas for vector potentials and current density (14), a component proportional to velocity and inversely proportional to the pulsation of the exciting current appeared:

$$j_s(\rho, z) = -\frac{\sqrt{2}Gi}{\delta}\left[\int_0^\infty \frac{k\psi(k)J_1(k\rho)e^{-kz}}{1-j\sqrt{2}\delta k}dk + j\frac{v}{\omega}\int_0^\infty \frac{k^2\psi(k)J_1(k\rho)e^{-kz}}{1-j\sqrt{2}\delta k}dk\right] \tag{14}$$

where $\psi(k)$ is a function dependent on the radial current distribution, assumed a priori, and G is a geometry factor that is also dependent on this distribution.

However, in further calculations of magnetic induction and force, this component was omitted due to the negligible value of v/ω. On the basis of comparison with the results of experimental studies, the authors of [3,52] emphasized that the presented model gives correct results for high frequencies (f > 20 kHz) of the exciting current. Based on this simplified model, studies of mechanical and thermal phenomena in the IDD in reference [4] were continued.

Other analytical research includes the quasi-steady approach used by the authors of [61], where they solved the Helmholtz Equation (15) for harmonic extortion using the variable separation method assuming the majority of simplifications that were used in [52]:

$$\frac{\partial^2 A_\theta}{\partial r^2} + \frac{1}{r}\frac{\partial A_\theta}{\partial r} - \frac{A_\theta}{r^2} + \frac{\partial^2 A_\theta}{\partial z^2} = j\omega\mu A_\theta \tag{15}$$

However, it should be underlined that the applied quasi-steady approach is a far-reaching approximation, taking into account the damped nature of the impulse-generated coil field. The authors themselves admitted that they obtained a satisfactory compliance of simulation and experimental results only for low frequencies.

4.2. Development of Hybrid Circumferential-Field Models of IDD

When analyzing the possibilities and simplification of the above mentioned circumferential-field models, it should be noted once again that these models did not give a full and reliable distribution of magnetic field in the entire disc volume, mainly due to the lack of consideration of disc motion when determining the equivalent mutual coil–disc inductance, i.e., omitting the impact of this motion on electromagnetic phenomena. This is justified by the fact that under certain conditions (depending mainly on parameters such as the initial energy of the capacitor and the mass of the disc), the unsteady electromagnetic field fades before the disc starts to move. Therefore, the authors of the papers noted above [3,4,52,61] determined the electrodynamic force in a stationary system, and then on its basis the motion of the disc was determined. It seems, therefore, that in order to obtain a solution for a fully coupled system not only magnetically, but also mechanically, such a model cannot be solved with analytical methods.

The authors developed a model [35] that took into account the transient state of the phenomena occurring in the IDD, the magnetic coupling of the coil and disc (including disc motion), and the effect of this motion on the coil field, together with the variability of eddy current density in the entire disc. This (2D) model can be qualified as a circumferential or circumferential-field model, and the solution method in [35] was described by the authors as an analytical–numerical approach due to the application of an analytical formula of vector magnetic potential around a circular filament (also circular cross-section) with current (16):

$$A_\Theta = \frac{\mu_0 i}{2\pi}\sqrt{\frac{r_c}{r_p}}\left[\left(\frac{2}{k} - k\right)K(k) - \frac{2}{k}E(k)\right] \tag{16}$$

where: $k = 2 \cdot \sqrt{\frac{r_p \cdot r_c}{(r_p + r_c)^2 + (z)^2}}$

$K(k)$, $E(k)$—respectively, first- and second-order elliptical integrals;
r_c, r_p—respectively, coil-winding radius and disc filament radius;
z—distance between the coil and the disc.

This approach was possible owing to the discretization method [58–60] of both the disc and the coil (*current filament methodology* [62]), also assuming the cylindrical symmetry of the system (Figure 9). Using the analytical form of potential (16), it is possible to derive analytical formulas for both self-inductance and mutual inductance between particular circular filaments. The mutual inductance between the coil and disc filaments are already functions dependent on the disc displacement variable z (17).

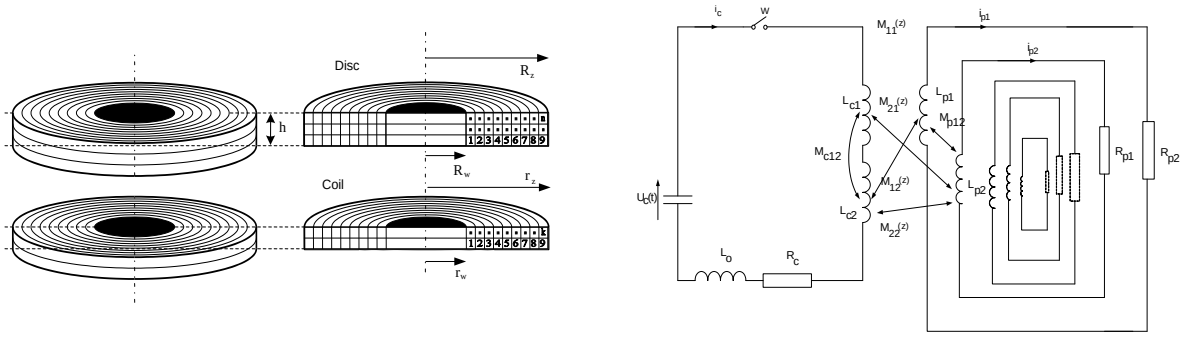

Figure 9. Discretization of the coil and disc and equivalent multi-loops circuit diagram of IDD.

Owing to the analytical form of mutual inductances, one can also obtain an analytical form of their derivatives (18). However, it should be emphasized that the obtained formulas can be considered as precisely defined values if the filament cross-section has the shape that is closest to circular. Therefore, discretization of the disc and coil was done for a square shape and had to be adequately dense. This condition hampered and, in fact, prevented the use of an uneven grid for this approach. Because of the analytical compounds thus obtained, the model was reduced to the numerical solution of the system of ordinary differential equations together with the attached equation of motion. This system, written in the matrix form, had to be brought back to the normal form, i.e., required the inversion of the main matrix. In the non-stationary case, the elements of this matrix are dependent on the coil–disc distance varying in time, hence the need to invert this matrix in every numerical step. If a stationary approach can be used for a given case, the calculation time is radically shortened not only due to the one-time inverse matrix calculation, but also due to the possibility of using the state variable method to solve the system.

$$M(z,i,j) = \mu_0 \sqrt{r_p(i) \cdot r_c(j)} \left[\left(\frac{2}{k(z,i,j)} - k(z,i,j) \right) \cdot K(k(z,i,j)) - \frac{2}{k(z,i,j)} \cdot E(k(z,i,j)) \right] \tag{17}$$

$$\frac{dM(z,i,j)}{dz} = \frac{\mu_0 \sqrt{r_p(i) \cdot r_c(i)} \cdot (z + d_z(i,j))}{\left(r_p(i) + r_c(i)\right)^2 + (z + d_z(i,j))^2} \cdot \left[\frac{2K(k(z,i,j))}{k(z,i,j)} - \frac{\left(2 - (k(z,i,j))^2\right) \cdot E(k(z,i,j))}{k(z,i,j) \cdot (1 - k(z,i,j))^2} \right] \tag{18}$$

As a result of solving the system of IDD model equations, the coil current and the currents of the disc filaments are determined in its entire volume without being limited only to the skin layer. The non-stationary variant also takes into account the effect of disc movement on the determined currents. The current density distribution allows for determining the forces acting on the individual filaments of the disc, which further allows for determining the pressure acting on the disc, which constitutes the input data for stress analysis. This model is dubbed by the authors as circumferential or field-circumferential with voltage extortion, where the field feature is the use of the solution of the field equation determining the vector's magnetic potential (16). The Mathcad environment was used to implement the model. The authors assumed the name ED for this original model and it

was further used for testing the IDD properties with different parameters, e.g., for different dimensions of a cylindrical disc. The results of these tests were presented and verified with experimental results [35,36] carried out using the new measurement system (Figure 4). As expected, in the case of "thick" discs in relation to the initial energy of capacitor banks, a very good convergence of results was obtained. The experiments also confirmed that even a slight change in the thickness of the disc reveals its elasticity and that means the need to use a mechanical model that determines the vibrations of the disc.

In summary, the ED model allows for the exact determination of electromagnetic quantities taking into account the motion of a rigid disc. However, the degree of accuracy is related to the degree of discretization and the numerical step in this procedure. Unfortunately, in the case of non-stationary division of up to 100 filaments, it extended computation time to many hours, which is a serious research difficulty. This is due to the fact that for the increasing frequency of the suppressed current resulting from RLC parameters and the degree of coupling of the disc to the coil, uniform discretization should increase if we want to keep similar numerical accuracy (iteration error = const.). Therefore, the authors continued their research to optimize the ED model. In [63], the IDD model was presented which is a combination of a modified ED model called CI in [63] with a field model called FI, for which the input data were the coil currents from the CI model. In the first approach, it was decided to speed up the numerical calculations of elliptical integrals, which in the CI model in the Mathcad environment are determined on the basis of the Romberg procedure. To this end, approximations of these integrals by Chebyshev's series were used. Simulation comparative studies have shown that already for five components of this series the results obtained in both cases are indistinguishable. Because the tested induction–dynamic drive in the authors' considerations is mainly dedicated to hybrid short-circuit breakers, in which sufficient interval between contact (in some cases) is about 2 mm, it was decided to examine the legitimacy of using a stationary approach (initially a motionless disc). This causes the main matrix to contain elements that are independent of time and it is only inverted once in the numeric procedure.

In addition, instead of explicit methods (Runge–Kutta), one can apply a discrete procedure of state variables. Comparative tests of coil and disc currents along with forces and displacements obtained for stationary and non-stationary cases proved to be very similar, and in the case of displacement, the discrepancy of waveforms became apparent only from the third pulse of force. This fact confirms the usefulness of simulations carried out for stationary conditions, if the range of displacement is not more than a few millimeters. As a result of the research, it was found that the displacement range for which the use of a stationary case can be considered justified increases with decreasing the frequency of the coil current. Further simplification in the CI model to minimize computation time was based on the determination of a reduced disc—i.e., a truncated hypothetical disc for which the electrodynamic repulsive force generated from the coil remains virtually unchanged. An approximate dimension of the thickness (height) of the reduced disc could result from the estimation of the skin layer $\delta = 2/\sqrt{2\omega\mu_0\gamma_{Al}}$ based on the mean value of the current pulsation of the coil. However, it should be remembered that the occurring phenomena have a strongly suppressed transient character and that "trimming" (dimensional reductions) can also be made along the radius. For this purpose, the current density distribution in the disc should be determined for dense discretization. Hence, a stationary case was used for a reasonable calculation time.

In order to facilitate the determination of the optimal thickness and radial dimensions of the disc, on the basis of the obtained current density distribution in the entire disc volume, graphs of densities along the thickness and separately along the radius are determined. In the case considered in [63], it was possible to reduce the disc by as much as 50% both along the thickness and along the radius. In order to verify the correctness of the designated new disc dimensions, simulations were carried out for both (primary and reduced) discs also for both states (stationary and non-stationary), while for the comparison of displacement (in simulations) a constant mass value of both discs was assumed. Perfect compatibility

of all compared waveforms proved the legitimacy of determining a reduced disc, which significantly shortens the calculation time (while maintaining the same discretization density of the primary and reduced disc). The process of determining a reduced disc can also be treated as the optimal disc from the point of view of striving for the highest dynamics of the drive resulting from the ratio of generated force to the mass of the disc. However, it should be remembered that such optimization of the disc dimensions from the point of view of electromagnetic quantities (including electrodynamic force) does not have to lead to optimal dimensions from the point of view of the disc stress state. The distribution of the magnetic field and the resulting pressure acting on the disc were in [38] the input data for the mechanical model.

Because in the CI model the discretization did not exceed 100 filaments, the FLUX 3D environment (using FEM) was used to increase the accuracy of the current density distribution, in which the coil–disc system could only be modeled under current extortion, but the disc was divided (meshing) into 40,000 elements. As a consequence, a model was created consisting of a "combination" of CI and FI models (referred to in [63] as the CI-FI hybrid circumferential-field model). The block diagram of CI-FI coupled models is shown in Figure 10. As can be seen from this diagram, the coil current constituting current extortion for the field model is calculated on the basis of the CI model at the predetermined reduced disc. This current can be calculated for both stationary and non-stationary cases. Next, in the FI model, the current density distribution for the real (unreduced) disc is determined, and hence the resultant axial force as a function of time, also for a stationary case. On the basis of this force, displacement was determined for the real disc, still considered here as a moving element with non-vibrating translatory motion.

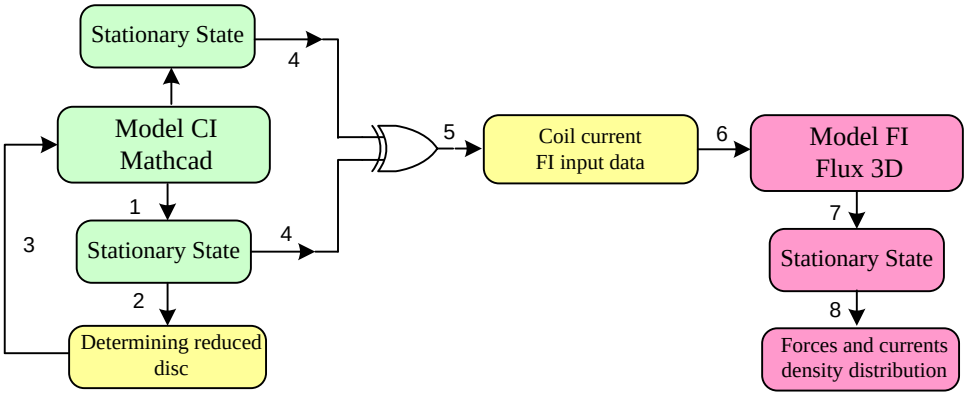

Figure 10. Block diagram of the hybrid circumferential-field model (CI-FI) with current extortion (1–8—sequences of execution of blocks).

Comparison of force simulations from the CI and CI-FI models and displacements with CI-FI and the experiment showed very good compliance, which confirms positive validation. When comparing the existing and even modified CI model with the new CI-FI, it should be emphasized that although the simulation time in CI, owing to the reduced disc determination even for the non-stationary case, decreased significantly, but with much higher discretization it would still require several hours (on a PC computer at that time). Meanwhile, the simulation time with a dense disc division (corresponding to this division in CI) in CI-FI was several minutes. The CI-FI model, because of its ability to accurately determine the current density in the entire disc area, and hence the volume forces, was used to analyze stresses in the mechanical model [34]. However, it should be emphasized that the approach used here is based on the adoption of a current extortion for the field model. If this extortion was specified in the CI even for the non-stationary case, then farther in CI-FI the effect of disc movement on the induction of additional EMF (EMF rotation) is omitted. However, as mentioned above, the authors of [3,52] assumed the validity of omitting the element containing the factor v/ω in Formula (14).

Additionally, the comparative simulation studies (CI for non-stationary state vs. CI-FI) confirmed the negligible effect of disc motion on the induction of EMF rotation because, due to the small range of displacement needed (less than 3 mm), the velocity v does not exceed 10 m/s with pulsations above 10,000 rad/s. However, it should be remembered that with the increase in capacitor bank capacitance or/and the number of coil windings (i.e., increasing the inductance), the current pulsing in the IDD system decreases.

Summarizing the models described in this historical sketch, it should be noted that their development was further inspired by the advancement in the physical realizations of these actuators. Namely, the possibility of obtaining increasingly higher currents from modern capacitor batteries (hundreds of kiloamperes) increased their dynamics at increasingly higher frequencies (even 10 kHz) of generated current. Thus, the first single-circuit models by Kesselring [2] gave decent accuracy of the simulated force for low frequencies (below 1 kHz). Further circuit models, taking into account the change in mutual inductance between the coil and the disk, no longer had frequency limitations, but required the symmetry of the system [35,57] and would be realized for the stationary case, and later for the non-stationary case, i.e., taking into account the effect of the disk motion on changes in the magnetic field. These initial circumferential models had both analytical and numerical realizations. The foundations of analytical considerations of what can be classified as initial field modeling were laid by Basu and Srivastava [3,4,52], who analyzed both electromagnetic and mechanical and thermal aspects in their works. These models, in addition to symmetry, assumed a priori a known current distribution in the disk. Since the advent of commercial environments based on FEM techniques, there has been development of hybrid models that are a combination of proprietary programs [35] in the circumferential part with the use of FEM programs in the field part [63]. These models already allowed reliable determination of eddy current distribution in the disk, although the first commercial FEM programs assumed current extortion. Therefore, what was still missing was a model that allows field analysis of electromagnetic phenomena for an object of any shape under natural extortion from a capacitor bank, i.e., voltage extortion. Such a model was presented by the authors in [40].

4.3. Full 2D/3D Realizations of Electrodynamic Phenomena Occurring in IDD in an FEM-Based Environment

In order not to take into account the abovementioned limitations, there was further necessity to build a field model with voltage extortion taking into account the disc motion and its impact on all quantities in the entire process of the studied phenomenon. The environment selected for IDD modeling should enable such implementation, not only for objects characterized by cylindrical symmetry (2D), but also for 3D asymmetrical objects. Owing to the international RIDAM grant obtained by the authors, the *ANSYS* program package was purchased, which includes the electromagnetic package called *Maxwell*. Since IDD tests must also relate mechanical and thermal phenomena, the choice of this program seems to be suitable due to the possibility of data transfer from one (electromagnetic) model to a mechanical or thermal model within one environment (*ANSYS*).

Reference [40] presents the realization of electro-mechanical model called EL_M in 2D and 3D versions consisting of electromagnetic part realized in the *Maxwell* package and mechanical part in the *Transient Structural* package (both packages include *ANSYS*). The mechanical part is discussed in [40].

Maxwell's electromagnetic model is based on the solution of the general equation determining the vector magnetic potential (19). The velocity of the moving medium (disc) is determined on the basis of the equation of motion under the influence of electrodynamic force determined on the basis of the general formula (20), (in the CI circumpherential model, Formula (21) was used to determine the electrodynamic force). In addition, the model should be formulated with the coil power supply circuit from the capacitor battery, thus realizing the voltage extortion (Figure 11a). The model validation was carried out by comparing the results of the simulation with the results of the CI model for a non-stationary

case, which in turn was verified experimentally for IDD parameters, defined as *low energy* in [40].

$$\nabla \times \left(\frac{1}{\mu} \nabla \times \mathbf{A} \right) = \mathbf{J}_s - \sigma \frac{\partial \mathbf{A}}{\partial t} - \sigma \nabla V + \sigma \mathbf{v} \times \nabla \times \mathbf{A} \tag{19}$$

$$\mathbf{F}(t) = \iiint_{V_{disc}} \mathbf{J}(t) \times \mathbf{B}(t) dV_{disc} \tag{20}$$

$$F(t) = i_{coil} \cdot \sum_{i=1}^{n} \left(i_{disc\_fil_i} \sum_{j=1}^{k} \frac{dM_{ij}}{dz} \right) \tag{21}$$

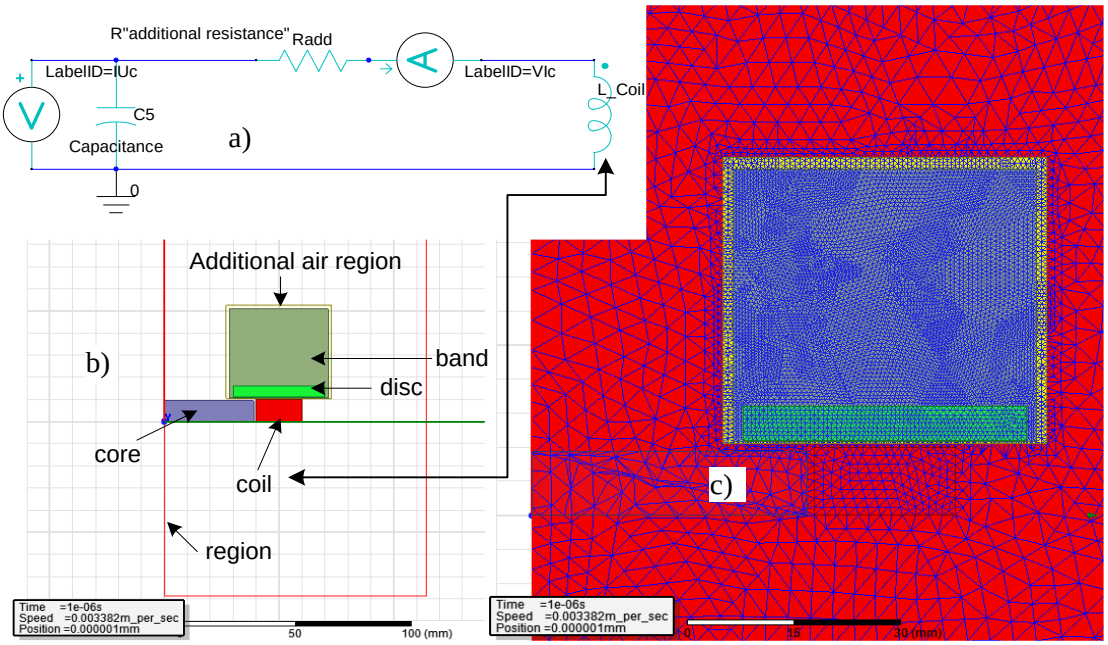

Figure 11. *Maxwell* EL model: (**a**) Thomson coil power circuit, (**b**) IDD objects, (**c**) discretization of objects.

In the first step, a 2D model was built, which still requires the modeled object to have features of cylindrical symmetry. Figure 11b shows the main screen of the model, in which the user draws cross-sections of the objects constituting the model (or more precisely, half of the cross-sections symmetrically in relation to the *z*-axis).

Figure 11b shows that the coil can be modeled taking into account the core, although it follows from the research conducted so far [4,52,56] that in order to obtain maximum drive dynamics, a coil with minimum inductance is preferred. It is sufficient to adopt an *air* environment for the core. In the electromagnetic part of the new model, for which [40] assumed the name EL, it is possible to take full account of the impact of disc motion on electromagnetic phenomena by placing the moving disc in the area called *band* (Figure 11b,c). The program allows for formulating motion parameters such as the mass of the moving element (disc), damping, and the initial value of the speed. The resultant force under the influence of which the disc moves is continuously determined on the basis of Formula (20). It is important to determine the movement limit that must be contained within the *band* area.

The main advantage of the 2D model in relation to 3D is the calculation time, which also in the case of modeling the movement of the disc for 3D models can be significant (hours). However, in both types of models (2D and 3D), a stranded object can be used to model the coil, which also significantly shortens the calculation time. However, it should be emphasized that the program for this type of coil does not even determine the DC resistance value (the user must specify it as an additional parameter R_{add}—circuit, from Figure 11a). The dynamically changing coil resistance (or rather the resistance of the coil

supply circuit considering the dynamic transition process) was determined experimentally for the previous models on the basis of the course with the disc immobilized or lack of disc. From the classical theory of solving an RLC circuit for an oscillatory case, it follows that by determining the first two pulses (the first and second maximum current = I, I3) of the transient current and the time T between them, the value of resistance and inductance can be determined by analytically solving a system of equations (Equation (22)) with a known capacity C of capacitor battery:

$$\frac{4\pi^2}{T^2} = \frac{1}{LC} - \left(\frac{R}{2L}\right)^2 \qquad T\frac{R}{2L} = \ln\left(\frac{I}{I3}\right) \tag{22}$$

In tested cases, this resistance may differ from the DC resistance by an order of magnitude. Another approach used, e.g., in [2,3,52,57], was to determine the DC resistance, but to do it for a reduced cross-section of the cable, taking into account the skin effect. This method was used by the authors of [39]. Capacitance is a preset parameter (specified by the manufacturer—checked by measurement also in the dynamic discharge state by a specified resistance). The inductance of the *stranded* coil is determined by the EL model. The inductance of the coil (apart from the above result obtained from (22)) can also be determined on the basis of an analytical formula determining the inductance of a single filament using Formula (16) and the mutual inductance between them using Formula (17). Owing to the small value of the air coil inductance, it is necessary to take into account the internal inductance of the wires. Very good preliminary validations of the newly developed model were obtained by comparing the inductance calculated on the basis of the analytical formula with the inductance determined by the EL model. In addition to the drive components, it is very important to determine the appropriate area of air surrounding the drive called the *region* in the *Maxwell* environment (Figure 11b). As a result of simulation studies, it turned out that the size of this region, especially when using the classical boundary condition (angular component of vector potential at its edges A = 0) has significant influence on the results. The comparison of the inductance of an analytically determined coil with the inductance determined by EL for a *stranded* coil made it possible to select an appropriate *region* size. In the examined case, in [40], the region of about 300% size in relation to the other elements made both inductances equal. In a situation where the region may turn out to be so large that the growing calculation time becomes uncomfortably long, *Maxwell's* environment offers a boundary condition called *balloon*, which assumes that the components of vector magnetic potential go to zero in infinity. As a result, the magnetic flux lines are neither perpendicular nor tangential to the virtual *region*. Simulation studies carried out for these two different types of conditions showed very good compatibility of the results with an area twice as small for the *balloon* case. When choosing a simulation step, one can choose the *adaptive* time step in the *Maxwell* environment. This option turned out to be ineffective if the initial step was incorrectly selected.

Therefore, to determine simulation parameters such as the numerical step and the density of the grid, convergence tests of the selected quantity were carried out (the maximum and minimum value of the coil current was selected (Figure 12)). Subsequent iterations shown in Figure 12 are simulations for the steps $h_{i+1} = 0.5h_i$, with the first initial step having the same value as in the circumferential model CI. Observing the convergence of waveforms from Figure 12, it should be noted that there should be no noticeable differences between simulation results obtained, e.g., in the sixth and previous iterations. The degree of compaction of the grids defined for individual objects (coil, disc, region) was also tested for convergence. It is recommended to "set up" an additional air area around the *band* object, which improves meshing in the area of motion, in which the mesh density has the greatest impact on the convergence of simulated quantities. In the *Maxwell* environment, it is possible to set up a grid with the skin effect in mind. The value of the skin layer should be given as a parameter in *Maxwell*. However, the generated mesh, for example, on a disc, determines such a layer around the whole object, which in the case under consideration is not justified.

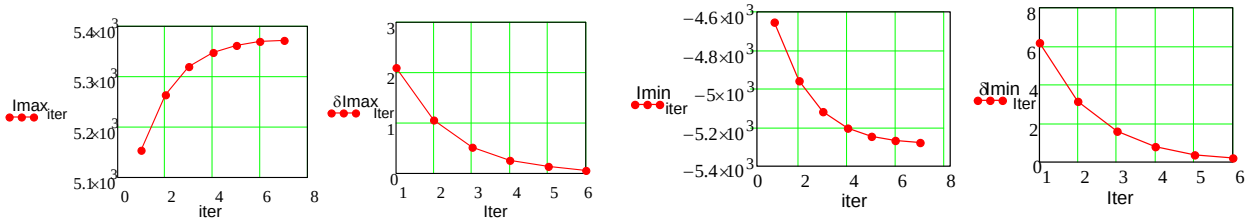

Figure 12. Convergence of the maximum and minimum values of the coil current and relative error.

Eventually, various mesh densities for individual elements were adopted, with the densest for the disc and *band* area. A sufficient, total number of elements for the (2D) case examined in [40] was approx. 8000. The final validation consisted in comparing the simulation results from the circumferential model CI and the new EL model for the numerical step determined at the sixth iteration. A comparison of all possible waveforms such as coil current, displacement, disc speed, and resultant axial force (for CI calculated on the basis of (21)) showed excellent compatibility. Despite the need to set a step 64 times smaller for the simulation in the EL (in relation to the step in CI) to achieve similar convergence, the simulation time (with the same discretization) was many times smaller. Another undoubted advantage of the EL (2D) model in relation to CI is the ability to design a disc and coil with any kind of cross-sectional shape. In turn, the post-processor capabilities of this type of environment enable determination, easy visualization, and animation of other selected quantities based on simulation results. In [38], the size of the radial forces that could possibly stiffen the disc during its vibrating motion was analyzed. Observations of the animation for both the vector magnetic field (magnetic induction) and as a consequence of the forces acting on the disc elements (Figure 13) unequivocally confirm the conclusion, which was obtained in [38] about the insignificances of these components. Figure 13 presents the screens of disc motion animation along with the forces acting on individual elements of the disc. Owing to the animation, it was observed that during the disappearance of the first pulse of force there appear (small) braking forces (Figure 13i–k). The sense of the instantaneous force of interaction between coil and disc filament can be explained on the basis of Formula (21), from which it appears that it depends on the shift between the currents (coil and a given disc filament) and the derivative of the mutual inductance in the instantaneous distance of the disc from the coil. However, the authors are not familiar with any publication showing a similar simulation result proving that during the movement there may appear forces whose resultant force will also have a sense opposite to the movement of the disc.

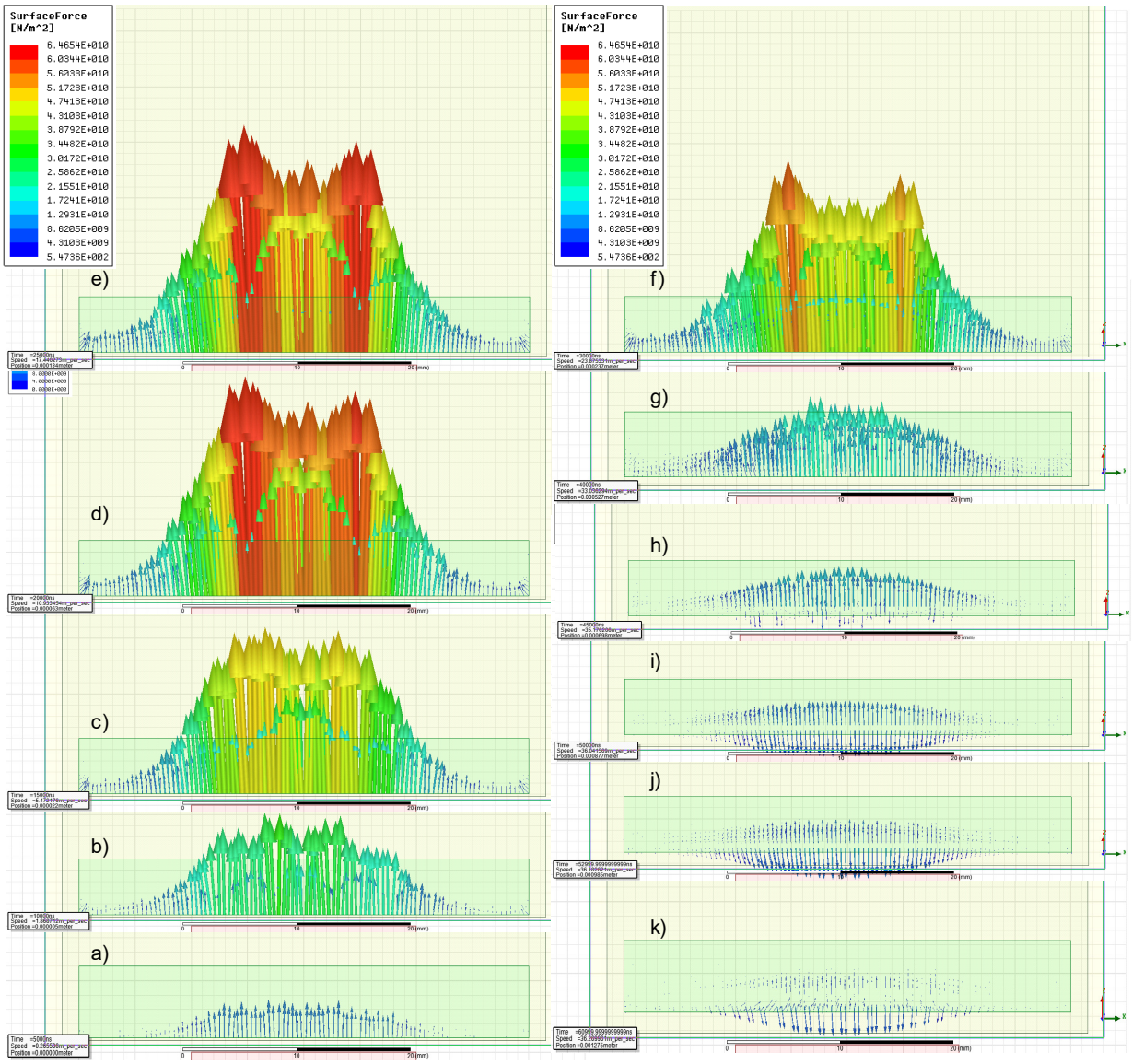

Figure 13. Screenshots of motion animation and of forces acting on each disc element: (**a**–**e**) increasing forces, (**f**–**k**) decreasing forces.

So far, this phenomenon (negative acceleration) has been observed in disc displacement registration (Figure 7b) or acceleration using a piezoelectric sensor [61], but it was assumed that this effect is caused only by vibrations of the measurement system and the disc itself. Summarizing the EL 2D model, it should be emphasized that in addition to the assumption of cylindrical symmetry of the modeled objects, the use of a *stranded* coil assumes the same instantaneous current density at each cross-sectional point of each turn. The coil which is modeled as *solid* does not have this type of assumption, where each turn is a separate object, but all are connected in series in one winding based on the external circuit modeled in the *Maxwell Circuit Editor* (Figure 14). However, when modeling every coil winding, one needs to be aware of the longer simulation time.

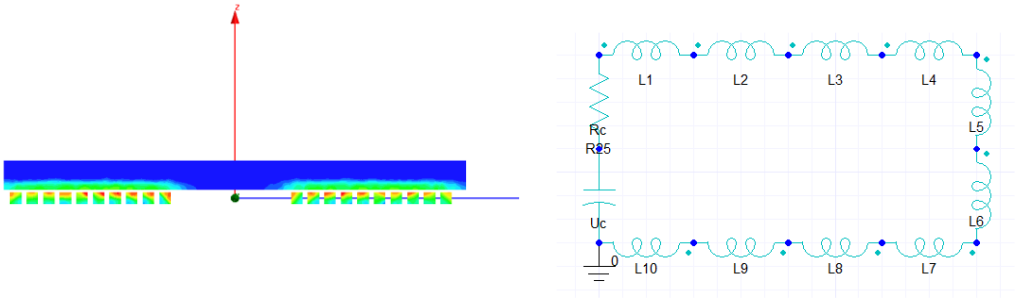

Figure 14. Drive model with *solid* coil and its external power supply circuit.

For testing the drive that has no symmetry, one has to use the 3D model. In order to check the correctness of constructing such a model, first, a symmetrical 3D model was built, the results of which are compared with the 2D model discussed above [40]. When modeling objects in a three-dimensional system, identical steps are performed as in the case of 2D models. The only exception is the determination of boundary conditions that the *Maxwell* environment sets automatically (for 3D), without the need for user intervention. The determination of additional air areas in addition to the *region* (around the *band* area) is also recommended to optimize the mesh. Furthermore, to minimize calculation time, the disc is divided into additional areas with thicknesses proportional to the estimated value of the skin layer (0.5δ, 1δ, 1.5δ . . .), forcing an uneven division (denser) of the disc into elements, counting from the surface closer to the coil. For the purpose of comparison with the 2D model, a *stranded* coil was also used and an identical integration step was adopted (as in 2D).

Assuming the number of elements into which all model objects were divided (disc, coil, region with areas) to be about 200,000, very good compatibility was obtained between the simulation results and the results obtained from the 2D model. The relative difference at any point of any waveform (current, displacement, force) did not exceed 1.5%, and the simulation time was around 2.5 h. Of course, calculation time can be reduced by using symmetry of the system and modeling, for example, only its quarter (Figure 15a).

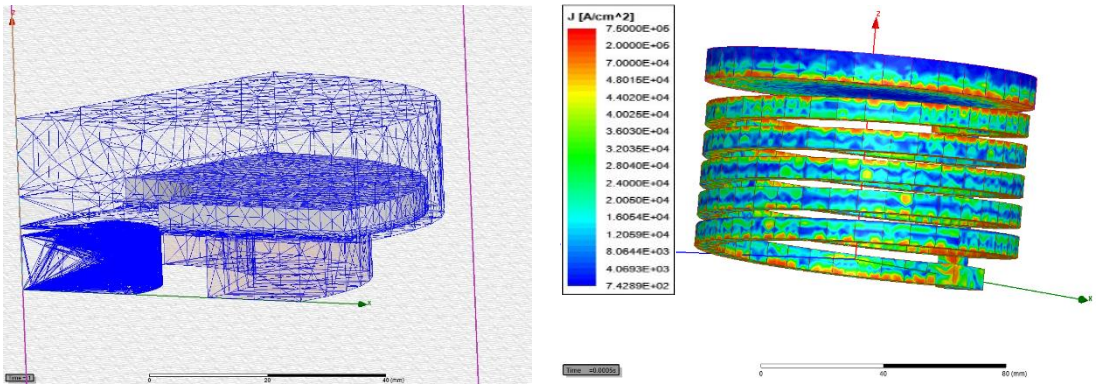

(**a**) (**b**)

Figure 15. Three-dimensional IDD model: (**a**) meshing of the quarter of the symmetrical system; (**b**) IDD with an asymmetrical cylindrical solid coil.

However, it should be remembered that animation of field results are then be able to be observed for this selected fragment, which may not give a satisfactory visual effect. Comparative tests were carried out for data at low initial energy and at very high initial energy [40], at which one should expect a clear deformation of the disc. In both cases, a very good similar consistency was obtained without altering the parameters of the model. The 2D and 3D models discussed were used to create a model coupled with a mechanical model called EL-M [40].

The final (universal) model, which does not have to have any symmetry, is a 3D model in which a *solid* coil is used. In Figure 15b, a model is shown in which the pitch of the cylindrical coil is taken into account. The model with a solid coil was used to study the thermal phenomena discussed in [41].

5. Conclusions

This article presents the historical development of induction–dynamic drive (actuators) research mainly in terms of electrodynamic phenomena with the omission of thermal and elastic phenomena.

The initial models required many simplifications, which could be omitted with the development of environments that also allow modeling of increasingly complex systems in 3D, that is, those that do not require any symmetry. The authors also presented their own full electrodynamic models that also take into account the effect of disc motion on the occurrence of electromagnetic phenomena. In summary, we separate our achievements into a model part and a research part. In the modeling part, we consider as our novelty the creation of a complete three-dimensional model that does not have to assume any simplifications concerning symmetry, stationarity, current forcing, among many others, which previous models, including ours, have assumed. In the research part, we consider as our novelty the observation, unpublished until now, of the negative return of the axial resultant force acting on the disc (Figure 13).

Most of the work shows that it is legitimate to ignore thermal and elastic phenomena if the drive is to meet the essential feature of cooperation in a hybrid switch system, which is repeatability. This means that the vibration of the disc must be elastic in nature, i.e., the permissible stresses must not be exceeded. In turn, due to the very short time of movement over a very short distance, the problem of heating can also be neglected if the circuit breaker does not operate in the automatic reclosing system. The authors have analyzed the endurance and thermal phenomena in [40,41]. From a design point of view, owing to the authors' recent own models presented here, it is now possible to design very precisely an actuator that cooperates synchronously with the hybrid circuit breaker system. The authors, as already mentioned, have realized multi-models in which models for mechanical and thermal analysis have been combined under the assumption of the so-called weak coupling, which, given the short distance that is needed when working with a hybrid switch, is reasonable. It is worth noting, however, that another challenge will be to create a drive model in which all three phenomena mentioned are fully coupled (strong coupling—such work is currently unknown to the authors). It will then be possible to design switches in which the secondary element constituting the current contact will not move as a rigid body, but will deform, which can further reduce the opening time of the switch. In the experimental field, the development of a measuring system that allows recording temperature fading after a few milliseconds is anticipated. Measurement of such adiabatic ultra-fast heating and cooling is unknown to the authors.

Author Contributions: P.J.: Conceptualization, Methodology, Software, Validation, Formal analysis, Investigation, Resources, Writing—original draft, Writing—review and editing, and Visualization. D.H.: Methodology, Formal analysis, Writing—review and editing, Supervision, Project administration, and Funding acquisition. J.M.: Conceptualization, Investigation, and Writing—review and editing. K.J.: Conceptualization, Validation, Resources, and Writing—review and editing. M.N.: Conceptualization and Validation. M.W.: Conceptualization, Validation, and Resources. All authors have read and agreed to the published version of the manuscript.

Funding: This research received no external funding.

Data Availability Statement: The data presented in this paper are available upon request from the corresponding author. The data are not publicly available due to concerns about the possible use of Maxwel_Ansys models and Mathcad's codes (designed by the corresponding author) without permission preserving the authors' copyright.

Conflicts of Interest: The authors declare that they have no known competing financial interests or personal relationships that could have appeared to influence the work reported in this paper.

References

1. Karpenko, L.N. *Fast-Acting Electrodynamic Disconnecting Devices*; Energy Leningrad: Leningrad Oblast, Russia, 1980.
2. Kesselring, F. Controlled Synchronous Circuit Breaker. *Electrotech. J. Germany, A* **1967**, *24*, 593–598.
3. Basu, S.; Srivastava, K.D. Analysis of A Fast Acting Circuit Breaker mechanism Part I: Electrical Aspects. *IEEE Trans. Power Appar. Syst.* **1972**, *PAS-91*, 1197–1203. [CrossRef]
4. Basu, S.; Srivastava, K.D. Analysis of A Fast Acting Circuit Breaker mechanism Part II: Thermal and Mechanical Aspects. *IEEE Trans. Power Appar. Syst.* **1972**, *PAS-91*, 1203–1211. [CrossRef]
5. Bissal, A.; Magnusson, J.; Engdahl, G. Electric to Mechanical Energy Conversion of Linear Ultrafast Electromechanical Actuators Based on Stroke Requirements. *IEEE Trans. Ind. Appl.* **2015**, *51*, 3059–3067. [CrossRef]
6. Peng, C.; Huang, A.; Husain, I.; Lequesne, B.; Briggs, R. Drive Circuits for Ultra-fast and Reliable Actuation of Thomson Coil Actuators used in Hybrid AC and DC Circuit Breakers. In Proceedings of the 2016 IEEE Applied Power Electronics Conference and Exposition (APEC), Long Beach, CA, USA, 20–24 March 2016.
7. Peng, C.; Husain, I.; Huang, A.Q.; LeQuesne, B.; Briggs, R. A Fast Mechanical Switch for Medium Voltage Hybrid DC and AC Circuit Breakers. *IEEE Trans. Ind. Appl.* **2016**, *52*, 2911–2918. [CrossRef]
8. Peng, C.; Husain, I.; Huang, A.Q. Evaluation of Design Variables in Thompson Coil based Operating Mechanisms for Ultra-Fast Opening in Hybrid AC and DC Circuit Breakers. In Proceedings of the 30th IEEE Annual Applied Power Electronics Conference and Exposition 2015, Charlotte, NC, USA, 15–19 March 2015.
9. Park, S.H.; Jang, H.J.; Chong, J.K.; Lee, W.Y. Dynamic analysis of Thomson coil actuator for fast switch of HVDC circuit breaker. In Proceedings of the Electric Power Equipment Switching Technology (ICEPE_ST), Busan, Republic of Korea, 25–28 October 2015; pp. 425–430.
10. Rodak, M.; Borkowski, P. Magnetic field analysis of the Inductive Dynamic Drive. *Electr. Rev.* **2018**, *94*, 47–50. [CrossRef]
11. Peng, C. Active Damping of Ultrafast Mechanical Switches for Hybrid AC and DC Circuit Breakers. *IEEE Trans. Ind. Appl.* **2017**, *53*, 5354–5364. [CrossRef]
12. Stroehla, T.; Dahlmann, M.; Sattel TKellerer, T. A Model of an Ultra -Fast Moving Magnet Actuator for Power Switches in Medium Voltage Grids. In Proceedings of the 2018 X International Conference on Electrical Power Drive Systems (ICEPDS), Novocherkassk, Russia, 3–6 October 2018; pp. 1–6. [CrossRef]
13. Sattarov, R.R.; Enikeev, R.D.; Razyapov, M.V. Dynamics of Fast-Switching Electrodynamic Actuator for Fuel Injection in Internal Combustion Engines. In Proceedings of the 2019 Dynamics of Systems, Mechanisms and Machines (Dynamics), Omsk, Russia, 5–7 November 2019; pp. 1–6. [CrossRef]
14. Maierhofer, J.; Rixen, D.J. Development of an Electrodynamic Actuator for an Automatic Modal Impulse Hammer. In *Dynamic Substructures*; Linderholt, A., Allen, M., D'Ambrogio, W., Eds.; Conference Proceedings of the Society for Experimental Mechanics Series; Springer: Cham, Switzerland, 2021; Volume 4. [CrossRef]
15. Zvolský, T. Power consumption of electrodynamic valve actuator. In Proceedings of the 25th International Conference Engineering Mechanics, Svratka, Czech Republic, 13–16 May 2019; pp. 423–426. [CrossRef]
16. Stroehla, T.; Dahlmann, M.; Kellerer, T.; Wagner, T.; Wagner, N.; Sattel, T. Ultra-fast moving coil actuator for power switches in medium-voltage grids. *J. Eng.* **2019**, *2019*, 4085–4089. [CrossRef]
17. Menne, H. Novel Ultra-Fast Drive Concept Based on Bi-Stable Disc Springs for use in Hybrid HVDC Circuit Breakers. Doctoral Dissertation, ETH Zurich, Switzerland, 2021.
18. Jankowski, P. Investigation of Features of Inductive Dynamic Drive. Ph.D. Thesis, Gdansk Technical University, Gdansk, Poland, 1998.
19. Barry, N. Dynamic of Jumping Rings and Collars. *Int. Elect. Enging. Educ.* **1998**, *35*, 357–369. [CrossRef]
20. Alferov, D. DC vacuum circuit-breaker. Discharges and Electrical Insulation in Vacuum. In Proceedings of the ISDEIV 2008, International Symposium on Discharges and Electrical Insulation in Vacuum, Bucharest, Romania, 15–19 September 2008; Volume 1. [CrossRef]
21. Meyer, J.M.; Rufer, A. A DC hybrid circuit breaker with ultra-fast con-tact opening and integrated gate-commutated thyristors (IGCTs). *IEEE Trans. Power Deliv.* **2006**, *21*, 646–651. [CrossRef]
22. Mokhberdoran, A.; Carvalho, A.; Silva, N.; Leite, H.; Carrapatoso, A. A new topology of fast solid-state HVDC circuit breaker for offshore wind integration applications. In Proceedings of the 17th European Conference on Power Electronics and Applications (EPE'15 ECCE-Europe), Geneva, Switzerland, 8–10 September 2015; pp. 1–10.
23. Nguyen, V.-V.; Son, H.-I.; Nguyen, T.-T.; Kim, H.-M.; Kim, C.-K. A novel topology of hybrid HVDC circuit breaker for VSC-HVDC application. *Energies* **2017**, *10*, 1675. [CrossRef]
24. Chen, Z.; Yu, Z.; Zhang, X.; Wei, T.; Lyu, G.; Qu, L.; Huang, Y.; Zeng, R. Analysis and Experiments for IGBT, IEGT, and IGCT in Hybrid DC Circuit Breaker. *IEEE Trans. Ind. Electron.* **2018**, *65*, 2883–2892. [CrossRef]
25. Zhang, X.; Yu, Z.; Zeng, R.; Huang, Y.; Zhao, B.; Chen, Z.; Yang, Y. A State-of-the-Art 500-kV Hybrid Circuit Breaker for a dc Grid. *IEEE Ind. Electron. Mag.* **2020**, *14*, 15–27. [CrossRef]
26. Kim, H. Gate Drive Controller for Low Voltage DC Hybrid Circuit Breaker. *Energies* **2021**, *14*, 1753. [CrossRef]

27. Atmadji, A.M.S.; Sloot, J.G.J. Hybrid Switching a Review of Current. In Proceedings of the International Conference on Energy Management and Power Delivery, EMPD 2, Singapore, 5 March 1998; pp. 683–688. [CrossRef]
28. Czucha, A.; Woloszyn, J.; Woloszyn, M. The comparison of ultra fast A.C. hybrid circuit breakers with GTO and IGBT. In Proceedings of the 35th Universities Power Engineering Conference UPEC'2000, Belfast, UK, 6–8 September 2000.
29. Czucha, J.; Jankowski, P.; Pikoń, M.; Żyborski, J. Ultra rapid contact member with arcless current commutation. In Proceedings of the International Conference on Electrical Contacts, Electromechanical Components and their Applications ICECT'99, Nagoya, Japan, 19–24 July 1999.
30. Jakubiuk, K.; Jankowski, P.; Woloszyn, J. Commutation of current in A.C. hybrid circuit breaker. In Proceedings of the XXIII Seminar on Fundamentals of Electrotechnics and Circuit Theory, Ustroń, Poland, 24–27 May 2000; pp. 313–316.
31. Ahn, H.; Lee, J.; Lee, B.; Hahn, S. Optimal design of permanent magnet actuator for vacuum circuit breakers using response surface methodology. *Int. J. Appl. Electromagn. Mech.* **2015**, *45*, 503–509. [CrossRef]
32. Lebkowski, A. Analysis of the Use of Electric Drive Systems for Crew Transfer Vessels Servicing Offshore Wind Farms. *Energies* **2020**, *13*, 1466. [CrossRef]
33. Jawale, R.; Govind, K. Hybrid circuit breaker–an uninterrupted solution for single bus system. *Int. Res. J. Mod. Eng. Technol. Sci.* **2021**, *3*, 1853–1859.
34. Jankowski, P.; Mindykowski, J.; Woloszyn, M. Effect of Power frequency on the stress state of disc actuator. *Int. J. Appl. Electromagn. Mech. IJAEM* **2014**, *45*, 639–647. [CrossRef]
35. Jankowski, P. Analytic-numerical approach in modelling electrodynamic phenomena of inductive dynamic drive. *J. Chin. Inst. Eng.* **2016**, *39*, 79–86. [CrossRef]
36. Jankowski, P.; Mindykowski, J. Measurement of quantities characterizing the properties of an inductive dynamic drive. *Electr. Rev.* **2012**, *88*, 78–82.
37. Jankowski, P.; Mindykowski, J.; Dudojć, B. Simple method of dynamic displacement record of contacts driven by inductive dynamic drive. *Metrol. Meas. Syst.* **2009**, *16*, 5–18.
38. Jankowski, P. Modelling of magnetoelastic phenomena In inductive dynamic driver. *J. Electr. Eng. Technol. (JEET)* **2017**, *12*, 1073–1081. [CrossRef]
39. Jankowski, P.; Mindykowski, J. Study on the Hazard Limitation of Hybrid Circuit Breaker Actuator Operation. *Energies* **2018**, *11*, 416. [CrossRef]
40. Jankowski, P.; Woloszyn, M. Comparison of properties of the new electro-mechanical model and circumferential model of the inductive-dynamic drive. *Int. J. Appl. Electromagn. Mech. IJAEM* **2019**, *59*, 483–494. [CrossRef]
41. Jankowski, P.; Woloszyn, M. Study of the effect of adiabatic heating on the operation of the electrodynamic actuator. *Int. J. Appl. Electromagn. Mech. IJAEM* **2019**, *59*, 495–504. [CrossRef]
42. Bartosik, M.; Lasota, R.; Wójcik, F. Arcless D.C. Hybrid Circuit Breaker. In Proceedings of the International Symposium on Switching Arc Phenomena SAP&ETEP, Łódź, Poland, 3–6 September 1997; pp. 115–119.
43. Czucha, J.; Pikoń, M.; Żyborski, J. Ultra rapid IGBT-contact current limiting interrupting device of very high breaking capacity. In Proceedings of the 8th International Symposium on Short Circuit in Power Systems, SCC'98, Brussels, Belgium, 8–10 October 1998.
44. Lasota, R. The work of hybrid switches in low voltage direct current circuits. In Proceedings of the Fifth International Symposium on Switching Arc Phenomena, Łódź, Poland, 24–26 September 1985.
45. Kim, H. Capacitor Commutation Method for MVDC Hybrid Circuit Breakers. *Designs* **2021**, *5*, 28. [CrossRef]
46. Woloszyn, J. Analysis of Critical Parameters of Superfast A.C Hybrid Circuit Breaker in the Proces of Current Shutdown. Ph.D. Thesis, Gdansk University of Technology, Gdansk, Poland, 2001.
47. Nowacki, W. *Electromagnetic Effects in Solid Deformable Bodies*; PWN: Warsaw, Poland, 1983.
48. Nowacki, W. *Theory of Elasticity*; PWN: Warsaw, Poland, 1970.
49. Sikora, R. *Electromagnetic Field Theory*; PWN: Warsaw, Poland, 1997.
50. Hryńczuk, J. *Theory of the Magneto-Thermo-Elastic Explosion Mechanism of a Wire Subjected to a High Power Current Shock, Warsaw Institute of Fluid-Flow Machinery*; PWN: Warsaw, Poland, 1966.
51. Jakubiuk, K. *Mechanism of Striatal Disintegration of Exploding Wires*; PG 510; Gdańsk Scientific: Gdansk, Poland, 1992.
52. Basu, S.; Srivastava, K.D. Electromagnetic Forces on a Metal Disc in Alternating Magnetic Field. *IEEE Trans. Power Appar. Syst.* **1969**, *PAS-88*, 1281–1285. [CrossRef]
53. Ziętek, B. *Optoelectronics*; UMK: Torun, Poland, 2011; ISBN 978-830-231-2746-8.
54. Jankowski, P. About the lack of convergence in an environment with limited representation of the number. *Electrotech. Rev.* **2016**, *1*, 20–23. [CrossRef]
55. Jankowski, P.; Młyński, A.; Wołoszyn, J. Data Approximation in Mathcad Environment. In Proceedings of the International Conference on Fundamentals of Electrotechnics and circuit theory IC-SPETO Ustroń 2010, Ustron, Poland, 26–29 May 2010.
56. Pasek, Z.; Mastny, V. *Efficienty of a Certain Class of Electrodynamic Drives for Electrical Apparatuses*; Z.94; Electrotechnics Institute: Warsaw, Poland, 1964.
57. Lubowa, L.L.; Siwkow, A.P. The Mathematical Model of the Actuator with Capacitive Power Supply. *Electromechanics* **1973**, *9*, 950–958.
58. Andrews, J.A.; Devine, J.R. Armature design for coaxial launchers. *IEEE Trans on Mag.* **1991**, *27*, 639–643. [CrossRef]

59. Azzerboni, B.; Cardelli, E.; Tellini, A. Analysis of magnetic field distribution in an homopolar generator as a pulse power source of electromagnetic accelerator. *IEEE Trans. Magn.* **1988**, *24*, 495–499. [CrossRef]
60. Elliot, D.G. Mesh-Matrix Method for Electromagnetic Launchers. *IEEE Trans. Magn.* **1989**, *25*, 164–169. [CrossRef]
61. Rajotte, R.; Drouet, M. Experimental Analysis of Fast Acting Circuit Breaker Mechanism-Electrical Aspects. *IEEE Trans. Power Appar. Syst.* **1975**, *94*, 89–96. [CrossRef]
62. Azzerboni, B.; Cardelli, E.; Raugi, M.; Tellini, A. Some remarks on the current filament modeling of electromagnetic launchers. *IEEE Trans. Magn.* **1993**, *29*, 643–648. [CrossRef]
63. Jankowski PWołoszyn, M. Suitability study of hybrid model of electrodynamic actuator. *Int. J. Appl. Electromagn. Mech. IJAEM* **2014**, *45*, 649–657. [CrossRef]